

1 Seasonal characterization of CDOM for lakes in semi-arid regions of
2 Northeast China using excitation-emission matrices fluorescence and
3 parallel factor analysis (EEM-PARAFAC)

4 Ying Zhao¹, Kaishan Song^{1*}, Zhidan Wen¹, Lin Li², Shuying Zang³, Tiantian Shao¹,

5 Sijia Li¹, Jia Du¹

6 ¹Northeast Institute of Geography and Agroecology, Chinese Academy of Sciences,
7 Changchun, Jilin, 130102, China

8 ²Department of Earth Sciences, Indiana University-Purdue University, Indianapolis,
9 IN, USA

10 ³College of Geographical Science, Harbin Normal University, Harbin, China

11 *corresponding author E-mail: songks@iga.ac.cn; Tel: 86-0431-85542364

12
13 **Abstract.** The seasonal characteristics of fluorescent components in CDOM for lakes
14 in the semi-arid region of Northeast China were examined by excitation-emission
15 matrix (EEM) spectra and parallel factor analysis (PARAFAC). Two humic-like (C1
16 and C2) and the protein-like (C3 and C4) components were identified using
17 PARAFAC. The average fluorescence intensity of the four components differed under
18 seasonal variation from June and August 2013 to February and April 2014.
19 Components 1 and 2 exhibited a strong linear correlation ($R^2 = 0.633$). Significantly
20 positive linear relationships between CDOM absorption coefficients $a(254)$ ($R^2 = 0.72$,
21 0.46 , $p < 0.01$), $a(280)$ ($R^2 = 0.77$, 0.47 , $p < 0.01$), $a(350)$ ($R^2 = 0.76$, 0.78 , $p < 0.01$)
22 and F_{max} for two humic-like components (C1 and C2) were exhibited, respectively. A

23 significant relationship ($R^2 = 0.931$) was found between salinity and DOC. However,
24 almost no obvious correlation was found between salinity and EEM-PARAFAC
25 extracted components except for C3 ($R^2 = 0.469$). Results from this investigation
26 demonstrate that the EEM-PARAFAC technique can be used to evaluate the seasonal
27 dynamics of CDOM fluorescent components for inland waters in the semi-arid
28 regions of Northeast China, and to quantify CDOM components for other waters with
29 similar environmental conditions.

30 **Keywords:** CDOM, fluorescent components, EEMs, PARAFAC, DOC, Salinity

31
32

33 **1 Introduction**

34 Dissolved organic matter (DOM), a heterogeneous mixture of humic acids,
35 proteins and carbohydrates, plays important roles in aquatic ecosystems (Zhang et al.,
36 2010). Chromophoric dissolved organic matter (CDOM), the colored fraction of
37 DOM, absorbs light energy in the ultraviolet (UV) and visible region of the spectrum
38 and inhibits the propagation of UV radiation. CDOM in waters also affects the
39 transport and bio-availability of materials such as trace metals and other pollutants
40 (Song et al., 2013), so it can be used as a proxy of water quality. In natural water
41 bodies, CDOM originates from the degradation of plant materials and other organisms
42 and terrestrially imported substances, which varies in time and space and is controlled
43 by its structure and composition (Stedmon et al., 2003). CDOM is compositionally
44 complex, making it difficult to isolate hydrophobic from hydrophilic acids using XAD
45 ion-exchange resins (Aiken et al., 1992; Spencer et al., 2010). Nonetheless, some

46 optically active components of CDOM can emit fluorescence after absorbing light at
47 certain wavelengths (Zhang et al., 2010) so that the fluorescence spectroscopic
48 techniques can be used to provide detailed information about the source and
49 concentration of CDOM. The traditional fluorescence techniques including
50 fluorescence emission spectrometry and synchronous fluorescence scanning applied
51 to examine CDOM components have the drawback that the output was restricted to a
52 linear scan (Hudson et al., 2007).

53 Recently, excitation-emission matrix fluorescence spectroscopy (EEM) has been
54 applied to identify CDOM components because of its ability to produce synchronous
55 scan spectra in the form of contours (Stedmon et al., 2003; Zhang et al., 2010). The
56 EEM spectroscopy is considered the most effective technique for studying the
57 composition of fluorophores given its high selectivity and sensitivity to CDOM in
58 water columns (Zhang et al., 2010). In recent years, EEM spectroscopy has been
59 widely used to investigate the dynamics of marine, freshwater and ice-water
60 ecosystems as well as snow melting water (Barker et al., 2006, 2009, 2010, 2013;
61 Coble, 2007; Fellman et al., 2010; Guo et al., 2010; Hudson et al., 2007; Stedmon et
62 al., 2007). Moreover, the EEM spectroscopy can also be used to distinguish
63 allochthonous and autochthonous CDOM sources in aquatic environments (Coble et
64 al., 1998; Mayer et al., 1999; Yamashita et al., 2008, 2010; Zhang et al., 2013). Based
65 on the peak positions in EEMs, two main fluorescent components, i.e., humic-like and
66 protein-like substances, have been identified and investigated (DelCastillo et al., 1999;
67 Jaffe' et al., 2004). However, overlapped fluorophores of CDOM EEMs could make

68 this traditional ‘peak-picking’ method unreliable to evaluate CDOM dynamics in
69 aquatic ecosystems (Coble, 1996; Stedmon et al., 2003). Recently, the combined
70 EEMs-PARAFAC (parallel factor analysis) technique has been shown to effectively
71 decompose EEM of CDOM into independent fluorescent components and assess the
72 source of CDOM and relationships with other water quality parameters. A number of
73 investigators have used EEMs-PARAFAC to characterize DOM in freshwater and
74 marine aquatic environments (Broisover et al., 2009; Cory et al., 2005; Guo et al.,
75 2010; Stedmon et al., 2003; Stedmon and Markager, 2005; Yamashita, 2008; Zhang et
76 al., 2010, 2011, 2013). Stedmon et al. (2003) introduced PARAFAC and identified
77 five distinct DOM components for a Danish estuary and its catchment. In coastal
78 environments, Yamashita et al. (2008) reported on seven components using the
79 combined EEMs-PARAFAC technique and assessed the dynamic of individual
80 fluorophores and their relationship with salinity in Ise Bay. Zhang et al. (2011) also
81 found three different components by PARAFAC modeling and analyzed the
82 correlations between the fluorescent components and absorption coefficients of
83 CDOM for Lake Tianmu and its catchment.

84 The Songnen Plain is a fluvial plain with semi-arid climate, in which many fresh
85 and brackish waters are distributed according to its geomorphological characteristics
86 (Song et al., 2013). Dissolved organic carbon (DOC) characteristics of these fresh
87 and brackish waters across the Songnen Plain have been studied by Song et al. (2013);
88 the results indicated that a huge amount of DOC was stored in these waters. In
89 particular, brackish waters would exhibit high average DOC concentrations and

90 significantly contributed the carbon budget to inland waters (Duarte et al., 2008; Song
91 et al., 2013; Tranvik et al., 2009). However, little study has been made on the detailed
92 information of DOC sources for these waters in the Songnen Plain. Therefore, it
93 motivated us to investigate the components in CDOM for both fresh and brackish
94 waters in the semi-arid region. In the present study, the absorption and fluorescence of
95 CDOM were determined for the water samples collected from seven lakes in the
96 western part of Jilin province, which varied at different seasons. The specific
97 objectives of this study are to: 1) characterize CDOM components contained in these
98 lakes using EEMs and their origins through the EEM-PARAFAC method; 2) assess
99 the dynamic of individual fluorescent components of CDOM under seasonal variation;
100 and most importantly 3) link CDOM fluorescence intensities, absorption coefficients,
101 DOC concentrations and salinity to each other, in order to establish proxies for
102 CDOM bioavailability and photoreactivity in waters.

103

104 **2 Materials and Methods**

105 **2.1 Lakes and water sampling**

106 The water bodies investigated in this study were located in the western part of Jilin
107 Province, which belongs to the semi-arid part of the Songnen Plain (Song et al., 2013).
108 Two groups of lakes were investigated, i.e., the Chagan lake group and the Yuelianghu
109 lake group. The Chagan lake group is made up of Lake Chagan (CGL), Xinmiaopao
110 (XMP), Xindianpao (XDP) and Kulipao (KLP). The Yuelianghu lake group mainly
111 includes Lake Yueliang (YLL), Talahong (TLH) and Xinhuangpao (XHP) (Fig. 1).

112 The two groups are about 60 km away from each other, of which each includes both
113 fresh and brackish waters. The primary economic value for these lakes is fisheries,
114 agricultural irrigation and recreation. The average annual precipitation is about 391
115 mm, but the average evaporation is up to 1790 mm, resulting in water scarcity. Due to
116 the area dominated by saline-alkali soil, the rainfall flush and agricultural catchment
117 land use can result in an increase of lake salinities. These seven lakes are endowed
118 with similar geological, hydrological and climatic settings, thus we presume that
119 similar processes may control the CDOM components. In order to characterize the
120 CDOM fluorescent components under seasonal variation using EEMs-PARAFAC, 67
121 water samples were collected from the surface of the seven lakes in 1-liter
122 acid-cleaned plastic bottles during four field campaigns in June and August 2013 as
123 well as in February and April 2014, respectively. These samples were collected during
124 the ice covering period using an ice drilling auger. The under-ice surface water was
125 coming up when a hole was drilled in the ice layer by the auger. The ice shavings
126 were collected in plastic bags and the under-ice surface water was collected in plastic
127 bottles. The collected samples were held on ice and immediately transported to the
128 laboratory in the Changchun City of Jilin province within 3-5 hours. In the laboratory,
129 these samples were filtered within 24 h and then kept at 4 °C until analysis within two
130 days. Latitude and longitude of each sample location were recorded *in situ* using a
131 Trimble Global Positioning System (GPS).

132

133 **Figure 1. Locations of the water sampling sites for 7 lakes in the western part of Jilin**
134 **province, Northeast China. a) Yueliang lake group: YLL, Yueliang Lake; XHP;**

135 **Xinhuangpao; TLH; Talahong; b) Chagan lake group: CGL, Chagan Lake; XDP,**
136 **Xindianpao; XMP, Xinmiaopao; KLP, Kulipao.**

137

138 **2.2 Analytical procedures**

139 To characterize the basic parameters of water quality, salinity was measured through a
140 DDS-307 electrical conductivity (EC) meter in the laboratory. Salinity was expressed
141 in the basis of the UNESCO practical salinity unit (PSU 1978). The pH was measured
142 using a PHS-3C pH meter at room temperature (20 ± 2 °C) in the laboratory. Water
143 turbidity was determined using the Shimadzu UV-2600PC UV-Vis dual beam
144 spectrophotometer with matching 3 cm quartz cells at room temperature (20 ± 2 °C)
145 with Milli-Q water as the reference (UV talk letter vol. 10,
146 <https://shimadzu.com.au/uv-talk-letter-volume-10>). To determine DOC concentrations,
147 water samples were filtered through 0.45 µm filters and then measured using a
148 Shimadzu TOC-5000 Analyzer and a 1.2 % Pt on silica catalyst at 680 °C. Potassium
149 hydrogen phthalate was used as a standard. The reproducibility of the analytical
150 procedure was within 2-3 % for the current study (APHA, 1998; Song et al., 2011).

151

152 **2.3 Absorption measurement**

153 In the laboratory, all the samples were filtered at low pressure, first through a
154 pre-combusted Whatman GF/F filter (0.7 µm), and then through a pre-rinsed 25 mm
155 Millipore membrane cellulose filter (0.22 µm) into glass bottles. Absorption spectra of
156 the samples were measured between 200 and 800 nm at 1 nm increments using the
157 Shimadzu UV-2600PC UV-Vis dual beam spectrophotometer with a 1 cm quartz

158 cuvette and Milli-Q water as reference. The absorption coefficient a_{CDOM} was
159 calculated from the measured optical density (OD) of the sample using Eq. (1):

$$160 \quad a_{CDOM}(\lambda) = 2.303 [OD_{(\lambda)} - OD_{(null)}] / \gamma \quad (1)$$

161 where γ is the cuvette path length (0.01 m) and the factor 2.303 converts from base 10
162 to base natural logarithm transformation. Some fine particles possibly remained in the
163 filtered solution (Babin et al., 2003; Bricaud et al., 1995), therefore it was necessary
164 to correct for scattering by fine particles and in this case, $OD_{(null)}$ is the average optical
165 density over 740-750 nm where the absorbance of CDOM can be assumed to be zero.

166 A CDOM absorption spectrum ($a_{CDOM}(\lambda)$) can be expressed as an exponential
167 function (Babin et al., 2003; Bricaud et al., 1995):

$$168 \quad a_{CDOM}(\lambda_i) = a_{CDOM}(\lambda_r) \exp[-S(\lambda_i - \lambda_r)] \quad (2)$$

169 where $a_{CDOM}(\lambda_i)$ is the CDOM absorption at a given wavelength λ_i , $a_{CDOM}(\lambda_r)$ is the
170 absorption estimate at the reference wavelength λ_r (440 nm), and S is the spectral
171 slope of the CDOM absorption. According to Helms et al. (2008), S is calculated by
172 fitting a linear model to the data over a wavelength range of 275 to 295 nm ($S1$) or
173 350 to 400 nm ($S2$). To eliminate the inter-laboratory variability, the slope ratio $S_R =$
174 $S1/S2$ is defined to indicate the molecular weight and photo-bleaching of CDOM
175 (Helms et al., 2008; Zhang et al., 2010).

176

177 **2.4 Three-dimensional fluorescence measurement**

178 The EEMs analysis of CDOM were conducted using a Hitachi F-7000 fluorescence
179 spectrometer (Hitachi High-Technologies, Tokyo, Japan) with a 700-voltage xenon

180 lamp. The scanning ranges were 200–450 nm for excitation, and 250–500 nm for
181 emission. Readings were collected in the ratio mode at 5 nm intervals for excitation,
182 and at 1 nm intervals for emission, using a scanning speed of 2400 nm min⁻¹. The
183 band-passes were 5 nm for both excitation and emission. A Milli-Q water blank of the
184 EEMs was subtracted to eliminate the water Raman scatter peaks (McKnight et al.,
185 2001; Stedmon et al., 2003; Zhang et al., 2010, 2011).

186 The inner-filter effect, which results from reabsorption and excitation of the
187 fluorescence itself, can reduce the fluorescence intensity by 5% (Larsson et al., 2007;
188 McKnight et al., 2001). In order to eliminate the inner-filter effect, the EEMs were
189 corrected for absorbance by multiplying each value in the EEMs with a correction
190 factor based on the assumption that the average path length of absorption of the
191 excitation and emission light is one-half length of the cuvette (McKnight et al., 2001;
192 Zhang et al., 2010). The correction function is expressed as follows:

$$193 \quad F_{corr} = F_{obs} \times 10^{(A_{ex}+A_{em})/2} \quad (3)$$

194

195 where F_{Corr} and F_{obs} are the corrected and uncorrected fluorescence intensities and A_{ex}
196 and A_{em} are the absorbance values at the respective excitation and emission
197 wavelengths.

198 The measured fluorescence intensity is dependent on the concentration of the
199 dissolved fluorophores in water bodies. Finally, the fluorescence intensities of all
200 samples' EEMs were normalized to the area under the Milli-Q water Raman peak
201 (λ_{ex} =350 nm, λ_{em} =371-428 nm) measured daily (Lawaetz and Stedmon, 2009). The

202 contour figures of the EEMs were plotted using the Matlab 10.0 software package
203 (Math Works, Natick Massachusetts, America).

204

205 **2.5 The PARAFAC modeling**

206 PARAFAC, a three-way method, is applied to decompose the CDOM fluorescence
207 into separate fluorescent signals (Andersen and Bro, 2003; Stedmon and Bro, 2008).
208 According to Stedmon and Bro (2008), a similar PARAFAC analysis is carried out in
209 the present study using the DOMFluor toolbox in MATLAB with the “N-way toolbox
210 for MATLAB” (Andersson et al., 2000). Before PARAFAC modeling, the excitation
211 wavelengths from 200 to 220 nm and the emission wavelengths from 250 to 300 nm
212 were deleted because of their poor quality. In order to remove the effect of Rayleigh
213 scatter on PARAFAC modeling, the missing values (NaN-Not a number) were
214 inserted in the regions ($Ex-20 \cong Em \cong Ex+20$ and $2Ex-20 \cong Em \cong 2Ex+20$; unit: nm)
215 which are significantly influenced by the first and second order scattering from the
216 measured spectroscopic data (Hua et al., 2007; Stedmon and Bro, 2008).

217 To determine the appropriate number of PARAFAC components, the split-half
218 validation procedure was executed to verify whether the model was valid by
219 comparing the emission and excitation loadings from each half (Stedmon and Bro,
220 2008). Split-half analysis is the most effective method for implementing the
221 PARAFAC models, in which the EEMs are randomly divided into four groups of
222 equal size, and then analyzed for two half splits (1-2 and 3-4 half) respectively. If the
223 correct number of components is chosen, the excitation and emission loadings from

224 the two groups should show the same shape and size (Bro, 1997, 1999). The
225 fluorescence intensity of every component was represented by F_{max} (Raman unit: nm^{-1})
226 (Stedmon and Markager, 2005).

227

228 **2.6 Statistical analysis**

229 Statistical analysis was conducted using the SPSS 16.0 software package (Statistical
230 Program for Social Sciences). Regression and correlation analysis was used to
231 describe the relationship between CDOM absorption coefficient, DOC concentration,
232 salinity and F_{max} . A model II-ANOVA was performed to determine seasonal
233 variability is higher than between-lake variability. The difference is considered to be
234 statistically significant when p -values are less than or equal to 0.05.

235

236 **3 Results and discussion**

237 **3.1 Water quality conditions**

238 The water quality parameters, i.e., pH, salinity, turbidity for the 67 water samples
239 collected from June 2013 to April 2014 in the western part of Jilin province are
240 displayed in Table 1. When the set of samples from various field trips was pooled
241 together, the waters had high pH values and high salt contents. The highest salinity
242 was present when the lakes were frozen in February 2014, whereas relatively constant
243 values (around 0.40 PSU) were exhibited in the other three seasons. Also the water
244 bodies were highly turbid. The highest turbidity was present in June 2013, and then
245 reduced in August 2013, and the lowest value was recorded in February 2014.

246 Compared with February 2014, the turbidity had almost no change in April 2014
247 (Table 1).

248

249 **Table 1. Mean value of water quality parameters from June 2013 to April 2014.**

250

251 **3.2 EEMs characterization of CDOM**

252 Based on the EEMs ‘peak picking’ technique, the key fluorescence peaks can be
253 observed in 67 water samples: two humic-like and two protein-like substances (Coble,
254 1996; Stedmon et al., 2003). The humic-like components are the mixture of aromatic
255 and aliphatic compounds-humic-like acids from terrestrial substances, and aquatic
256 humic-like substances of phytoplankton origin. With respect to the protein-like
257 components (i.e., tyrosine-like and tryptophan-like substance), they mainly consist of
258 dissolved amino acids. As an example, Fig. S1 displays the EEMs of samples from
259 lake Xindianpao at different seasons. The peaks comprise two humic-like
260 fluorescence peaks: one in the ultraviolet range (Ex/Em = 220-240/410-430 nm) and
261 the other in the visible range (Ex/Em = 300-340/410-450 nm) and the protein-like
262 fluorescence peaks: tyrosine-like (Ex/Em = 210-230, 270-280/310-330 nm) and
263 tryptophan-like (Ex/Em = 220-230, 280-300/350-370 nm).

264

265 In our study, four separate fluorescent components (Fig. 2a-d) and the
266 excitation and emission loadings (e-h) of the four components identified by
267 EEM-PARAFAC are summarized in Fig. 2 and Table 2. The first fluorescent

268 component (C1) was a biological degradation humic-like component comparable to
269 humic-like peaks (M and N) in marine and in phytoplankton degradation experiments
270 for inland waters (Coble, 1996; Zhang et al., 2009). Component 2 was consistent with
271 the humic-like peaks (A and C) defined by Coble (1996). Component 3 resembles the
272 tryptophan-like (T) component as found by Baker et al. (2004) and Hudson et al.
273 (2007). For component 4, it is likely related to tyrosine-like component (B) (Hudson
274 et al., 2007). Components 3 and 4 represent autochthonous semi-labile CDOM
275 associated with bacteria activity and phytoplankton degradation (Borisover et al.,
276 2009; Stedmon et al., 2003). Particularly, there was a shoulder at the excitation
277 wavelength 310-330 nm in component 3 and 330-340 nm in component 4, which may
278 be due to the residual Raman peaks in some water samples (Fig. 2c-d). In this study,
279 not all of the four components were present in all of the samples.

280

281 **Figure 2. The PARAFAC modeling output shows the contour plots of the four PARAFAC**
282 **fluorescent components (a-d) and excitation (black) and emission (red) loadings (e-h) of each**
283 **component. Fluorescence is in Raman units: nm⁻¹.**

284

285 **Table 2. Positions of the fluorescence maximum peaks of the four components identified by**
286 **PARAFAC modeling in the present study compared with those previously identified.**
287 **Secondary excitation maxim is given in brackets.**

288

289 **3.3 Temporal distribution of PARAFAC components**

290 These fresh and brackish water in Jilin province in northeast China are endowed with
291 similar geological, hydrological and climatic settings, thus it is presumed that similar

292 processes may control the CDOM components. When a model II-ANOVA using
293 season and lake as random effect factors was performed, it shows that the seasonal
294 variability ($F > F_{crit}$, $p < 0.05$) is higher than between-lake variability. Therefore, the
295 water samples from different lakes for every season were pooled together in order to
296 study the seasonal variation of the fluorescent components. As shown in Fig. 3a, the
297 average fluorescence intensity of the four components had seasonal variation. When
298 all the water samples at different seasons were pooled together, the average value of
299 total fluorescence intensity was $2.05 \pm 0.93 \text{ nm}^{-1}$, corresponding to the intensities of
300 0.71 ± 0.32 (C1), 0.33 ± 0.11 (C2), 0.50 ± 0.24 (C3), and 0.51 ± 0.26 (C4) nm^{-1} for
301 different components. These results can demonstrate that the fluorescence intensity
302 was dominated by C1, implying most of the CDOM for the seven inland lakes
303 originated from the degradation of phytoplankton and microorganisms. The
304 protein-like components (C3 and C4), related to bioavailability and microbial activity
305 of CDOM, had almost the same magnitude. At all four seasons, the fluorescent
306 component C2, which was terrestrially imported to water bodies, contributed less to
307 total fluorescence than the other three. The total fluorescence intensity differed under
308 seasonal variation, varying from $2.54 \pm 0.68 \text{ nm}^{-1}$ in June to $1.93 \pm 0.70 \text{ nm}^{-1}$ in
309 August 2013, and then increased to $2.34 \pm 0.92 \text{ nm}^{-1}$ in February and reduced to the
310 lowest $1.57 \pm 0.55 \text{ nm}^{-1}$ in April 2014 (Fig. 3c). The intensities of four fluorescent
311 components (i.e., 0.75 ± 0.17 (C1), 0.32 ± 0.06 (C2), 0.69 ± 0.24 (C3), and $0.77 \pm$
312 0.20 (C4) nm^{-1}) (Fig. 3d) from the samples collected in June 2013 exhibited similar
313 trends to that for the pooled data set. These values were higher than the seasonal

314 average except C2 ($0.32 \pm 0.06 \text{ nm}^{-1}$). This can be explained by enhanced activities
315 from plant degradation and microbial activities, but less terrestrial substances were
316 imported to the water bodies in June and therefore the fluorescence intensity of C2
317 was lower than the seasonal average. Compared to the fluorescence intensity in June,
318 the three fluorescence intensities (0.65 ± 0.14 (C1), 0.33 ± 0.16 (C3), 0.52 ± 0.36 (C4)
319 nm^{-1}) from the samples collected in August 2013 were reduced, but an increased value
320 was recorded for C2 ($0.42 \pm 0.05 \text{ nm}^{-1}$) (Fig. 3d). Especially, the fluorescence
321 intensities of two protein-like components showed an obvious difference. This can be
322 attributed to substantially increased precipitation up to 180 mm in July from June to
323 August 2013 (Fig. 3b) so that floods occurred when rainfall continued to increase in
324 August. Gradually, DOM contained in terrestrial CDOM was flushed by rainfall to the
325 lakes so that the C2 ($0.42 \pm 0.05 \text{ nm}^{-1}$) fluorescence intensity became higher. In
326 accordance with Cheng et al. 2010, the rainwater CDOM for this study was largely
327 characterized by protein-like components (Cheng et al., 2010). The fluorescence
328 intensity of the rainwater CDOM was very weak, and also the rainwater CDOM
329 contained much lower humic-like concentration (Fig. S2b). The intensities of the
330 other three components decreased because of dilution resulting from heavy rain and
331 relatively weak microbial decomposition of plants.

332 The highest C1 ($1.02 \pm 0.38 \text{ nm}^{-1}$) presented in February 2014, and the C2 (0.39
333 $\pm 0.12 \text{ nm}^{-1}$) intensity remained almost the same as that in August 2013. However, the
334 protein-like components indicated that the C3 ($0.57 \pm 0.25 \text{ nm}^{-1}$) intensity was higher
335 than the C4 ($0.35 \pm 0.17 \text{ nm}^{-1}$) intensity, which was opposite to the results from other

336 months (Fig. 3d). In cold winter, the surface waters formed a thick layer of ice
337 covering the lake waters. Because the ice cover reduced light penetration and
338 restricted gas exchange between the underlying water and atmosphere, vigorous
339 biological activity in the lakes would be reduced at low temperature and low light
340 level (Thomas K., 1983; Uusikiv et al., 2010; Wharton, et al., 1993). Although the
341 biological activity was very weak, there could still be a bit of production of C1 and
342 C3 in lake water. Also, dissolved materials were left in the underlying surface waters
343 and little terrestrial matter was imported to the lakes once covered by ice (Stedmon et
344 al., 2007). Therefore, the C1 and C3 in the water of the lakes beneath the ice layers
345 would be produced and accumulated simultaneously, whereas, the C2 remained the
346 same. Obviously, the fluorescence intensity of component 1 reached the highest value
347 for the winter samples. As shown in Fig. S2a, another striking feature for the winter
348 samples was that the fluorescence of CDOM in the ice was dominated by the
349 tyrosine-like C4 component, which is consistent with the findings of Barker et al.
350 (2009, 2013) and Stedmon et al. (2007). It showed that the C4 component was left in
351 the ice-cover when the lakes were frozen. Therefore, it is not surprising that the
352 intensity of component C4 for water beneath ice layers was reduced and the
353 concentrated C3 showed a much higher fluorescence intensity. In April 2014, the
354 intensities of four fluorescent components (0.47 ± 0.17 (C1), 0.25 ± 0.08 (C2), $0.40 \pm$
355 0.16 (C3), and 0.45 ± 0.13 (C4) nm^{-1}) (Fig. 3d) exhibited similar seasonal trends
356 though these values were much lower than the average. Our interpretation is that the
357 ice CDOM was characterized by tyrosine-like component (C4) (Fig. S2a), and the

358 fluorescence intensity of C4 contributed by the ice-melt water was very weak.
359 However, the underlying lake CDOM included both humic-like (C1 and C2) and
360 protein-like (C3 or C4) components. When the ice in the lakes melted into water with
361 warming weather and biological degradation and human activity was weak, the lake
362 CDOM was diluted by the ice-melted water and the fluorescence intensity would
363 reach to the lowest value in early spring.

364

365 **Figure 3. a) Seasonal average of F_{max} for EEM-PARAFAC components (C1, C2, C3 and C4)**
366 **for lakes in the western part of Jilin province; b) Monthly variation of rainfall for the lakes**
367 **in western part of Jilin province from April 2013 to February 2014; c) Seasonal variation of**
368 **the total fluorescence intensity at different seasons; d) Seasonal variation of the four**
369 **EEM-PARAFAC components at different seasons. The error bars represent one standard**
370 **deviation.**

371

372 **3.4 CDOM versus EEM-PARAFAC extracted components**

373 The concentration of DOC, CDOM absorption coefficients and the slope ratio S_R are
374 shown in Table 3. The DOC concentrations ranged from 10.03 to 56.60 mg L⁻¹ with
375 an average value of 37.60 ± 18.05 mg L⁻¹ during the period from June 2013 to April
376 2014, demonstrating a seasonal dynamics that can be attributed to hydrological,
377 climatic and landscape variations (Song et al., 2013). The highest average DOC
378 concentration (55.04 ± 20.00 mg L⁻¹) was present in February 2014 (ice-covered
379 period); whereas, relatively constant values of approximate 30 mg L⁻¹ were observed
380 in the ice-free season. The relative high DOC concentration in ice-free season was
381 caused by evapo-condensed effect due to the prolonged sunshine duration for the

382 lakes in the Songnen Plain. With respect to the higher DOC concentration in winter, it
383 can be attributed to the accumulated DOC left in the liquid phase when ice formation
384 took place, resulting in the higher DOC concentration in the underlying water
385 (unpublished material). Generally, the absorption coefficient $a(350)$ is used as a proxy
386 for characterizing CDOM concentration (Guo et al., 2010; Zhang et al., 2011), $a(280)$
387 is related to DOC biodegradation (McDowell et al., 2006), and $a(254)$ can be used to
388 characterize the optical properties of DOC aromaticity (Jaffe' et al., 2004; Weishaar et
389 al., 2003). The highest averaged CDOM absorption coefficients $a(350)$, $a(280)$, $a(254)$
390 were also present in February 2014, corresponding to the highest DOC concentration.
391 The S_R values of the two wavelength ranges (275-295 nm over 350-400 nm) were
392 used to represent DOM molecular weight (Helms et al., 2008). The lowest mean of S_R
393 was present in August 2013 suggesting the relatively weak microbial decomposition
394 of plants and lots of terrestrially imported substances through rainwash resulted in the
395 higher average molecular weight of DOC.

396

397 **Table 3. Mean values of DOC concentration and CDOM absorption coefficients groups at**
398 **different seasons. S_R : the slope ratio of $S_{275-295\text{nm}}$: $S_{350-400\text{nm}}$.**

399

400 When the whole data set ($N = 67$) was pooled together, there were significantly
401 positive linear relationships between $a(254)$, $a(280)$, $a(350)$ and F_{max} for two
402 humic-like components (C1 and C2), respectively, but mostly such correlations were
403 not observed for the protein-like components (Fig. 4a and b, Table 3). These results
404 were in accordance with previous investigations (Zhang et al., 2010, 2011).

405 Components 1 and 2 were strongly linearly correlated with each other ($R^2 = 0.633$)
406 (Fig. 4c), indicating that the concentrations of the two humic-like components were
407 controlled by common sources (Baker and Spencer, 2004). There was a weak
408 relationship ($R^2 = 0.051$) between the protein-like components (C3 and C4) possibly
409 because of a complex origin of CDOM such as rainfall in summer, ice in winter and
410 organic pollutants derived from domestic, agricultural and industrial sewerage, which
411 represent the complex origins of CDOM. However, there was almost no correlation
412 between the humic-like and protein-like components. The linkage of a fluorescence
413 signal to DOC was very complicated because of the seasonal impacts, i.e., increased
414 rainfall, algal blooms and ice-cover, which affect the DOC concentration. Due to both
415 steady and labile CDOM fluorescent components in DOC, the fluorescent signal
416 would change with the ratio of fluorescent and non-fluorescent CDOM components
417 (Henderson et al., 2009). A weak relationship ($R^2 = 0.42$) (Fig. 4d) was found between
418 DOC and component 3 likely from the decay of plants through microbial activity or
419 the pollution from human and animal wastes.

420 Different from the findings by Yamashita et al. (2008) for ocean water, this study
421 did not find obvious correlation between salinity and EEM-PARAFAC extracted
422 components with the exception of C3 ($R^2 = 0.469$) (Table 4 and Fig. 4f). The most
423 important finding for the water samples collected at different seasons from the
424 Songnen Plain is a significant relationship ($R^2 = 0.931$) between salinity and DOC
425 (Fig. 4e). This is because DOC is evapo-condensed from spring to autumn and
426 freeze-accumulated in winter in the semi-arid region. A prolonged sunshine duration

427 can result in an evapo-condensed DOC concentration in ice-free season. On the other
428 hand, the DOC is accumulated when the lakes freeze in winter leaving DOC in the
429 liquid phase.

430

431 **Table 4. Correlation coefficients (R) and significance levels (p) of the linear relationships**
432 **between CDOM absorption, DOC, salinity and fluorescent components.**

433

434 **Figure 4. Relationships between CDOM absorption coefficient a(350) with a) $F_{max}(C1)$, b)**
435 **with $F_{max}(C2)$, c) peak $F_{max}(C1)$ versus $F_{max}(C2)$, d) peak $F_{max}(C3)$ versus DOC, e) Salinity**
436 **versus DOC, f) Salinity versus $F_{max}(C3)$.**

437

438 **4 Conclusions**

439 A model II-ANOVA using season and lake as random effect factors shows that the
440 seasonal variability ($F > F_{crit}$, $p < 0.05$) is higher than between-lake variability. In this
441 study, the application of EEM-PARAFAC to characterize four fluorescent
442 components under seasonal variation in CDOM was presented with 67 water samples
443 collected from June 2013 to April 2014 in the semi-arid region of the Songnen Plain.
444 Two humic-like and the protein-like components were identified using the PARAFAC
445 modeling. The average fluorescence intensity of the four components differed under
446 seasonal variation from June 2013 to April 2014. The highest C1 1.02 nm^{-1} was
447 presented in February 2014 probably due to the condensed CDOM caused by ice
448 formation in winter. Especially in summer when quantities of rainfall take place and
449 in winter when water is frozen, the fluorescence intensity is dominated by
450 tyrosine-like components in rain and ice-melt water. Component 1 and 2 exhibited a

451 strong linear correlation ($R^2 = 0.633$). There were significantly positive linear
452 relationships between F_{max} and CDOM absorption coefficient $a(254)$ ($R^2 = 0.72, 0.46,$
453 $p < 0.01$), $a(280)$ ($R^2 = 0.77, 0.47, p < 0.01$), $a(350)$ ($R^2 = 0.76, 0.78, p < 0.01$) for two
454 humic-like components (C1 and C2), respectively. A weak relationship ($R^2 = 0.42$)
455 was found between DOC and component 3 from the decay of plants through
456 microbial activity or the pollution from human and animal wastes. However, almost
457 no obvious correlation was found between salinity and EEM-PARAFAC extracted
458 components except C3 ($R^2 = 0.469$), though the correlation was not as strong as with
459 DOC concentration. Most importantly, a significant relationship ($R^2 = 0.931$) was
460 found between salinity and DOC. In order to understand the biogeochemical effects
461 on the aquatic ecosystem, further study should be required to identify CDOM source
462 and assess physical/chemical, bioavailable and photoreactive transformation in
463 various lakes with larger saline gradients in the semi-arid region, Northeast China.

464

465 **Acknowledgements**

466 The research was jointly supported by the “One Hundred Talents” program from
467 Chinese Academy of Sciences and the National Natural Science Foundation of China
468 (No. 41471290). The authors thank Zhi Ding, Ying Guan, Lei Liu and Ming Wang for
469 their persistent assistance with both field sampling and laboratory analysis.

470

471 **References**

472 APHA/AWWA/WE F.: Standard Methods for the Examination of Water and
473 Wastewater, Washington, DC: American Public Health Association, 1998.

474 Aiken, G. R., McKnight, D. M., Thorn, K. A., and Thurman, E. M.: Isolation of
475 hydrophobic organic-acids from water using nonionic macro porous resins, *Org.*
476 *Geochem.*, 18, 567-573, 1992.

477 Andersen, C. M., and Bro, R.: Practical aspects of PARAFAC modeling of
478 fluorescence excitation-emission data, *J. Chemom.*, 17, 200-215, 2003.

479 Andersso, C. A., and Bro. R.: The N-way Toolbox for MATLAB, *Chemom. Intell.*
480 *Lab. Syst.*, 52, 1-4, 2000.

481 Babin, M., Stramski, D., Ferrari, G. M., Claustre, H., Bricaud, A., Obolensky, G.,
482 and Hoepffner, N.: Variations in the light absorption coefficients of
483 phytoplankton, nonalgal particles, and dissolved organic matter in coastal waters
484 around Europe, *J. Geophys. Res.*, 108, 3211-3230, 2003.

485 Baker, A., Ward, D., Lieten, Shakti H., Periera, R., Simpson, Ellie C., and Slater, M.:
486 Measurement of protein-like fluorescence in river and waste water using a
487 handheld spectrophotometer, *Water Res.*, 38, 2934-2938, 2004.

488 Baker, A., and Spencer, R. G. M.: Characterization of dissolved organic matter from
489 source to sea using fluorescence and absorbance spectroscopy, *Sci. Total*
490 *Environ.*, 333, 217-232, 2004.

491 Barker, J. D., Dubnick, A., Lyons, W. B., and Chin, Y. P.: Changes in Dissolved
492 Organic Matter (DOM) Fluorescence in Proglacial Antarctic Streams, *Arct.*

493 Antarct. Alp. Res., 45, 305-317, 2013.

494 Barker, J. D., Sharp, M. J., Fitzsimons, S. J., and Turner, R. J.: Abundance and
495 dynamics of dissolved organic carbon in glacier systems, *Arct. Antarct. Alp. Res.*,
496 38, 163–172, 2006.

497 Barker, J. D., Sharp, M. J., and Turner, R. J.: Using synchronous fluorescence
498 spectroscopy and principal components analysis to monitor dissolved organic
499 matter dynamics in a glacier system, *Hydrol. Processes*, 23, 1487–1500, 2009.

500 Barker, J. D., Klassen, J. L., Sharp, M. J., Fitzsimons, S. J., and Turner, R. J.:
501 Detecting biogeochemical activity in basal ice using fluorescence spectroscopy,
502 *Ann. Glaciol.*, 51, 47–55, 2010.

503 Borisover, M., Laor, Y., Parparov, A., Bukhanovsky, N., and Lado, M.: Spatial and
504 seasonal patterns of fluorescent organic matter in Lake Kinneret (Sea of Galilee)
505 and its catchment basin, *Water Res.*, 43, 3104-3116, 2009.

506 Bricaud, A., Babin, M., Morel, A., and Claustre, H.: Variability in the
507 chlorophyll-specific absorption coefficients of natural phytoplankton: Analysis
508 and parameterization, *J. Geophys. Res.*, 100, 13321–13332, 1995.

509 Bro, R.: PARAFAC tutorial and applications, *Chemom. Intell. Lab. Syst.*, 38, 149-171,
510 1997.

511 Bro, R.: Exploratory study of sugar production using fluorescence spectroscopy and
512 multi-way analysis, *Chemom. Intell. Lab. Syst.*, 46,133-147, 1999.

513 Cheng, Y. Y., Guo, W. D., Long, A. M., and Chen, S. Y.: Study on optical

514 characteristic of chromophoric dissolved organic matter in rainwater by
515 fluorescence excitation-emission matrix and absorbance spectroscopy (Article in
516 Chinese), *Spectrosc. Spect. Anal.*, 30, 2413-2416, 2010.

517 Coble, P. G.: Characterization of marine and terrestrial DOM in seawater using
518 excitation-emission matrix spectroscopy, *Mar. Chem.*, 51, 325–346, 1996.

519 Coble, P. G.: Marine optical biogeochemistry: the chemistry of ocean color, *Chem.*
520 *Rev.*, 107, 402-418, 2007.

521 Coble, P. G., Del Castillo, C. E., and Avril, B.: Distribution and optical of CDOM in
522 the Arabian Sea during the 1995 Southwest Monsoon, *Deep-Sea Res. part II*, 45,
523 2195–2223, 1998.

524 Cory, R. M., and McKnight, D. M.: Fluorescence spectroscopy reveals ubiquitous
525 presence of oxidized and reduced quinines in dissolved organic matter, *Environ.*
526 *Sci. Technol.*, 39, 8142-8149, 2005.

527 DelCastillo, C. E., Coble, P. G., Morell, J. M., Lopez, J. M., and Corredor, J. E.:
528 Analysis of the optical properties of the Orinoco River plume by absorption and
529 fluorescence spectroscopy, *Mar. Chem.*, 66, 35–51, 1999.

530 Duarte, C. M., Montes, C., Cole, J. J., Striegl, R. G., Melackand, J., and Downing, J.
531 A.: CO₂ emissions from saline lakes: A global estimate of a surprisingly large flux,
532 *J. Geophys. Res. Biogeosci.*, 113, G04041, 2008.

533 Fellman, J. B., Hood, E., and Spencer, R. G. M.: Fluorescence spectroscopy opens
534 new windows into dissolved organic matter dynamics in freshwater ecosystems:

535 A review, *Limnol. Oceanogr.*, 55, 2452-2462, 2010.

536 Guo, W. D., Xu, J., Wang, J. P., Wen, Y. G., Zhou, J. F., and Yan, Y. C.:
537 Characterization of dissolved organic matter in urban sewage using excitation
538 emission matrix fluorescence spectroscopy and parallel factor analysis, *J.*
539 *Environ. Sci.*, 22, 1728-1734, 2010.

540 Henderson, R. K., Baker, A., Murphy, K. R., Hambly, A., Stuetz, R. M., and Khan, S.
541 J.: Fluorescence as a potential monitoring tool for recycled water system: A
542 review, *Water Res.*, 43, 863-881, 2009.

543 Helms, J. R., Stubbins, A., Ritchie, J. D., Minor, E. C., Kieber, D. J., and Mopper, K.:
544 Absorption spectral slopes and slope ratios as indicators of molecular weight,
545 source, and photo bleaching of chromophoric dissolved organic matter, *Limnol.*
546 *Oceanogr.*, 53, 955–969, 2008.

547 Hua, B., Dolan, F., Mcghee, C., Clevenger, ThomasE., and Deng, B. L.: Water-source
548 characterization and classification with fluorescence EEM spectroscopy:
549 PARAFAC analysis, *Int. J. Environ. Anal. Chem.*, 87, 135-147, 2007.

550 Hudson, N., Baker, A., and Reynolds, D.: Fluorescence analysis of dissolved organic
551 matter in natural, waste and polluted waters – a review, *River Res. Appl.*, 23,
552 631–649, 2007.

553 Jaffe', R., Boyer, J. N., Lu, X., Maie, N., Yang, C., Scully, N. M., and Mock, S.:
554 Source characterization of dissolved organic matter in subtropical
555 mangrove-dominated estuary by fluorescence analysis, *Mar. Chem.*, 84, 195–210,

556 2004.

557 Larsson, T., Wedborg, M., and Turner, D.: Correction of inner-filter effect in
558 fluorescence excitation-emission matrix spectrometry using Raman scatter, *Anal.*
559 *Chim. Acta.*, 583, 357-363, 2007.

560 Lawaetz, A. J., and Stedmon, C. A.: Fluorescence Intensity Calibration Using the
561 Raman Scatter Peak of Water, *Appl. Spectrosc.*, 63, 936-940, 2009.

562 Mayer, L. M., Schick, L. L., and Loder, T. C.: Dissolved protein fluorescence in two
563 Maine estuaries, *Mar. Chem.*, 64, 171–179, 1999.

564 McDowell, W. H., Zsolnay, A., Aikenhead-Peterson, J. A., Gregorich, E. G., Jones, D.
565 L., Joërdmann, D., Kalbitz, K., Marschner, B., and Schwesig, D.: A
566 comparison of methods to determine the biodegradable dissolved organic
567 carbon from different terrestrial sources, *Soil Biol. Biochem.*, 38, 1933–1942,
568 2006.

569 Mcknight, D. M., Boyer, E. W., Westerhoff, P. K., Doran, P. T., Kulbe, T., and
570 Andersen, D. T.: Spectrofluorometric characterization of dissolved organic
571 matter for indication of precursor organic material and aromaticity, *Limnol.*
572 *Oceanogr.*, 46, 38–48, 2001.

573 Song, C. C., Wang, L. L., Guo, Y. D., Song, Y. Y., Yang, G. S., and Li, Y. C.: Impacts
574 of natural wetland degradation on dissolved carbon dynamics in the Sanjiang
575 Plain, Northeastern China, *J. Hydrol.*, 398, 26-32, 2011.

576 Song, K. S., Zang, S. Y., Zhao, Y., Du, J., Lin, L., Zhang, N. N., Wang, X. D., Shao, T.

577 T., Guan, Y., and Liu, L.: Spatiotemporal characterization of dissolved carbon
578 for inland waters in semi-humid/semiarid region, China, *Hydrol. Earth Syst.*
579 *Sci.*, 17, 4269-4281, 2013.

580 Spencer, R. G. M., Hernes, P. J., Ruf, R., Baker, A., Dyda, R. Y., Stubbins, A., and
581 Six, J.: Temporal controls on dissolved organic matter and lignin
582 biogeochemistry in a pristine tropical river, *J. Geophys. Res. Biogeosci.*, 115,
583 G03013, 2010.

584 Stedmon, C. A., and Bro, R.: Characterizing dissolved organic matter fluorescence
585 with parallel factor analysis: a tutorial, *Limnol. Oceanogr. Methods*, 6, 572-579,
586 2008.

587 Stedmon, C. A., and Markager, S.: Tracing the production and degradation of
588 autochthonous fractions of dissolved organic matter by fluorescence analysis,
589 *Limnol. Oceanogr.*, 50, 1415-1426, 2005.

590 Stedmon, C. A., Markager, S., and Bro, R.: Tracing dissolved organic matter in
591 aquatic environments using a new approach to fluorescence spectroscopy, *Mar.*
592 *Chem.*, 82, 239-254, 2003.

593 Stedmon, C. A., Thomas, D. N., Granskog, M., Kaartokallio, H., Papadimitriou, S.,
594 and Kuosa, H.: Characteristics of dissolved organic matter in Baltic coastal sea
595 ice: allochthonous or autochthonous origins? *Environ. Sci. Technol.*, 41,
596 7273–7279, 2007.

597 Thomas K. B.: Under Landfast ice, *Arctic*, 36, 328-340, 1983.

598 Tranvik, L. J., Downing, J. A., Cotner, J. B., Loiselle, S. A., Striegl, R. G., Ballatore, T.
599 J., Dillon, P., Finlay, K., Fortino, K., Knoll, L. B., Kortelainen, P. L., Kutser, T.,
600 Larsen, S., Laurion, I., Leech, D. M., McCallister, S. L., McKnight, D. M.,
601 Melack, J. M., Overholt, E., Porter, J. A., Prairie, Y., Renwick, W. H., Roland, F.,
602 Sherman, B. S., Schindler, D. W., Sobek, S., Tremblay, A., Vanni, M. J.,
603 Verschoor, A. M., Wachenfeldt, E. V., and Weyhenmeyer, G. A.: Lakes and
604 reservoirs as regulators of carbon cycling and climate, *Limnol. Oceanogr.*, 54,
605 2298–2314, 2009.

606 Uusikiv, J., Vahatal, A.V., Granskog, M.A., Sommaruga, R., 2010. Contribution of
607 mycosporine-like amino acids and colored dissolved and particulate matter to
608 sea ice optical properties and ultraviolet attenuation, *Limnol. Oceanogr.*, 55(2),
609 703–713.

610 UV talk letter vol. 10, 2013. <https://shimadzu.com.au/uv-talk-letter-volume-10>

611 Weishaar, J. L., Aiken, G. R., Bergamaschi, B. A., Farm, M. S., Fujii, R., and Mopper,
612 K.: Evaluation of specific ultraviolet absorbance as an indicator of the chemical
613 composition and reactivity of dissolved organic carbon, *Environ. Sci. Technol.*,
614 37, 4702– 4708, 2003.

615 Wharton, R. A., Jr., McKay, C. P., Clow, G. D., and Andersen, D. T.: Perennial ice
616 covers and their influence on Antarctic lake ecosystems, *Antarct. Res. Ser.*, 59,
617 53–70, 1993.

618 Yamashita, Y.: Assessing the dynamics of dissolved organic matter (DOM) in coastal
619 environments by excitation emission matrix fluorescence and parallel factor

620 analysis (EEM-PARAFAC), *Limnol. Oceanogr.*, 53, 1900-1908, 2008.

621 Yamashita, Y., Cory, R. M., Nishioka, J., Kuma, K., Tanoue, E., and Jaffe', R.,:
622 Fluorescence characteristics of dissolved organic matter in the deep waters of the
623 Okhotsk Sea and the northwestern North Pacific Ocean, *Deep Sea Res. Part II*,
624 57, 1478–1485, 2010.

625 Zhang, Y. L., Liu, X. H., Osburn, C. L., Wang, M. Z., Qin, B. Q., and Zhou, Y. Q.:
626 Photo bleaching response of different Source of Chromophoric Dissolved
627 Organic Matter Exposed to Natural Solar Radiation Using Absorption and
628 Excitation-Emission Matrix Spectra, *Plos one*, 8, e77515, 2013.

629 Zhang, Y. L., Yin, Y., Feng, L. Q., Zhu, G. W., Shi, Z. Q., Liu, X. H., and Zhang, Y. Z.:
630 Characterizing chromophoric dissolved organic matter in Lake Tianmuhu and its
631 catchment basin using excitation-emission matrix fluorescence and parallel
632 factor analysis, *Water Res.*, 45, 5110-5122, 2011.

633 Zhang, Y. L., Zhang, E. L., Yin, Y., VanDijk, M. A., Feng, L. Q., Shi, Z. Q., Liu, M. L.,
634 and Qin, B. Q.: Characteristics and sources of chromophoric dissolved organic
635 matter in lakes of the Yungui Plateau, China, differing in trophic state and
636 altitude, *Limnol. Oceanogr.*, 55, 2645-2659, 2010.

637 Zhang, Y. L., VanDijk, M. A., Liu, M. L., Zhu, G. W., and Qin, B. Q.: The
638 contribution of phytoplankton degradation to chromophoric dissolved organic
639 matter (CDOM) in eutrophic shallow lakes: Field and experimental evidence.
640 *Water Res.*, 43, 4685–4697, 2009.

641

642

643 Table 1. Mean value of water quality parameters from June 2013 to April 2014. Turb
644 denotes water turbidity; N denotes sampling numbers.

645

Sampling season	pH	Salinity (PSU)	Turb (NTU)	N
Jun.2013	8.54	0.40	166.20±108.73	15
Aug.2013	8.63	0.37	63.13±31.21	13
Feb.2014	8.35	0.70	21.33±15.87	17
Apr.2014	8.67	0.43	22.24±16.42	22
All	8.55	0.48	62.18±79.07	67

646

647

648

649

650

651

652

653

654

655

656

657

658

659

660

661

662

663

664

665

666

667

668 Table 2. Positions of the fluorescence maximum peaks of the four components
669 identified by PARAFAC modeling in the present study compared with those
670 previously identified. Secondary excitation maxima is given in brackets.

671

Component No	Ex _{max} (nm)	Em _{max} (nm)	Description and source	Components (Coble) and (Zhang)	Components (Stedmon and Markager)
C1	230 (300)	425	Marine humic-like (phytoplankton degradation)	M	6
C2	255 (350)	460	Terrstrial humic-like	A and C	1 and 4
C3	225 (290)	360	Autochthonous tryptophan-like	T	
C4	220 (275)	320	Autochthonous tyrosine-like	B	8

672 Fluorescence peaks were named as Components (Coble) and (Zhang) by Coble et al. (1996, 1998) and Zhang et al.
673 (2010, 2011), while as Components (Stedmon and Markager) by Stedmon and Markager (2005).

674

675

676

677

678

679

680

681

682

683

684

685

686

687

688

689

690

691 Table 3. Mean values of DOC concentration and CDOM absorption coefficients

692 groups at different seasons. S_R : the slope ratio of $S_{275-295nm} : S_{350-400nm}$.

693

Sampling season	a(254) m ⁻¹	a(280) m ⁻¹	a(350) m ⁻¹	S_R	DOC mg L ⁻¹	N
Jun.2013	38.39±9.23	25.98±6.38	5.73±1.68	1.29±0.16	31.84±14.67	15
Aug.2013	29.71±4.73	19.36±2.91	5.82±0.81	0.96±0.22	32.83±14.78	13
Feb.2014	52.88±18.13	34.62±11.54	6.36±2.17	1.18±0.11	55.04±20.00	17
Apr.2014	34.43±11.38	22.45±7.36	4.17±1.49	1.32±0.13	30.86±10.91	22
All	39.08±14.73	25.73±9.58	5.40±1.84	1.21±0.20	37.60±18.05	67

694

695

696

697

698

699

700

701

702

703

704

705

706

707

708

709

710

711

712

713 Table 4. Correlation coefficients (R) and significance levels (*p*) of the linear
714 relationships between CDOM absorption, DOC, salinity and fluorescent components.

715

	a(254)	a(280)	a(350)	DOC	Salinity	C1	C2	C3	C4
DOC	0.711**	0.646**	0.294*	1.000**					
Salinity	0.650**	0.579**	0.159	0.965**	1.000**				
C1	0.850**	0.875**	0.873**	0.496**	0.383**	1.000**			
C2	0.677**	0.686**	0.885**	0.414**	0.270*	0.796**	1.000**		
C3	0.452**	0.417**	0.134	0.648**	0.685**	0.267*	0.103	1.000**	
C4	-0.040	-0.016	0.078	-0.101	0.135	0.084	0.069	0.225	1.000**

716 ***p*< 0.01 level ; **p*<0.05 level.

717

718

719

720

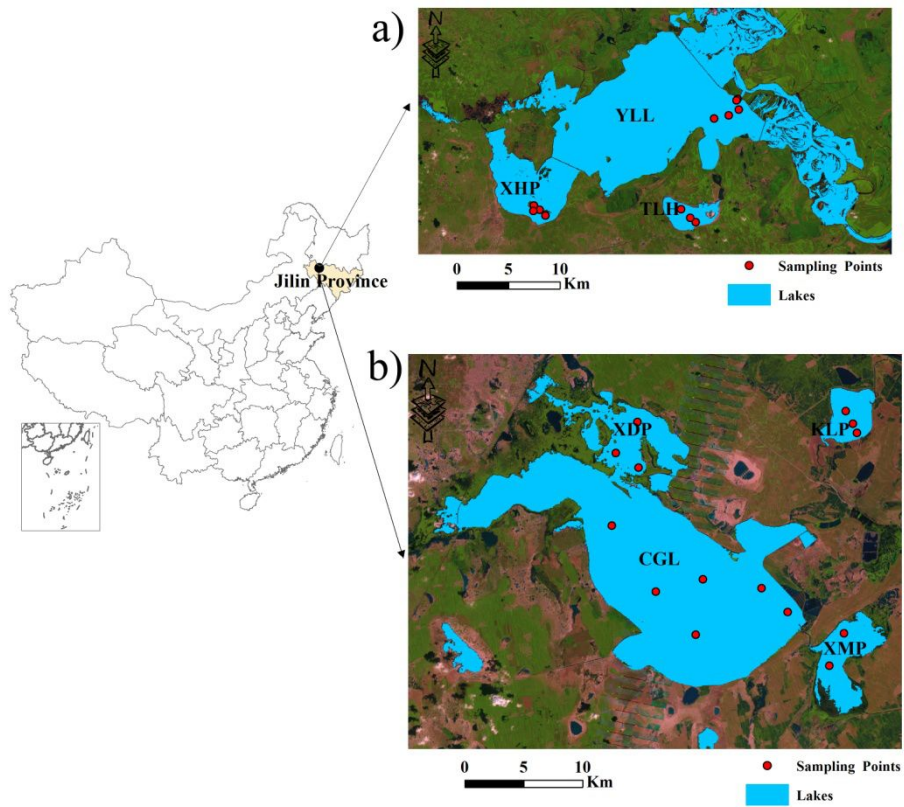
721

722

723

724

725



726

727 Figure 1. Locations of the water sampling sites for 7 lakes in the western part of Jilin
 728 province, Northeast China. a) Yueliang lake group: YLL, Yueliang Lake; XHP;
 729 Xinhuangpao; TLH; Talahong; b) Chagan lake group: CGL, Chagan Lake; XDP,
 730 Xindianpao; XMP, Xinmiaopao; KLP, Kulipao.

731

732

733

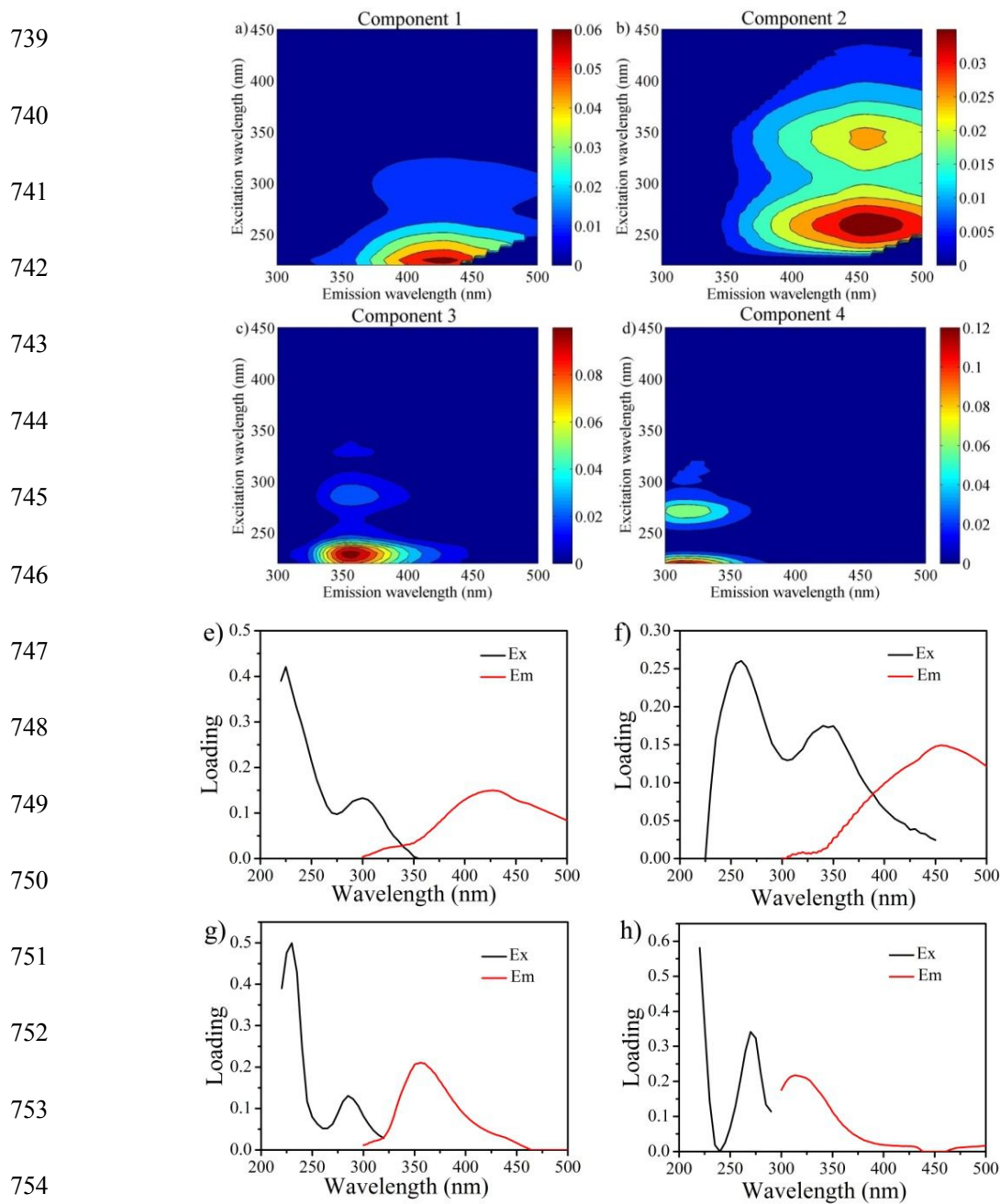
734

735

736

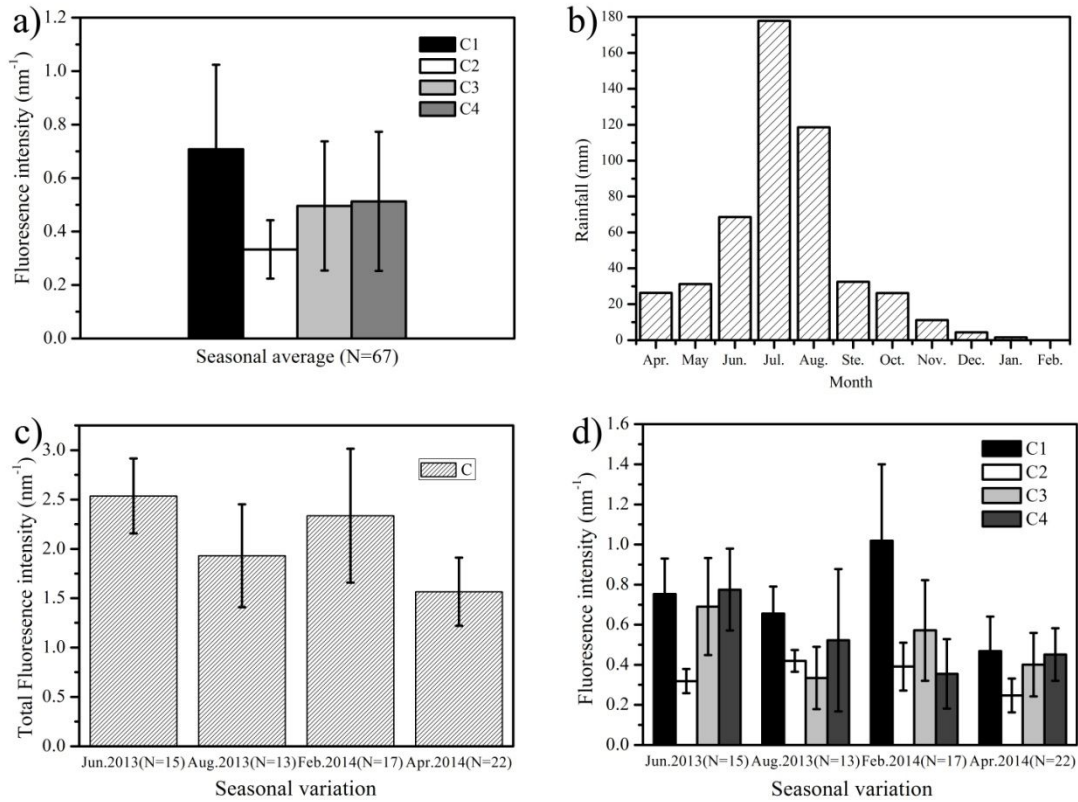
737

738



755 Figure 2. The PARAFAC model output shows the contour plots of the four
 756 PARAFAC fluorescent components (a-d) and excitation (black) and emission (red)
 757 loadings (e-h) of each component. Fluorescence is in Raman units: nm⁻¹.

758



759

760 Figure 3. a) Seasonal average of F_{max} for EEM-PARAFAC components (C1, C2, C3

761 and C4) for lakes in the western part of Jilin province; b) Monthly variation of rainfall

762 for the lakes in western part of Jilin province from April 2013 to February 2014; c)

763 Seasonal variation of the total fluorescence intensity at different seasons; d) Seasonal

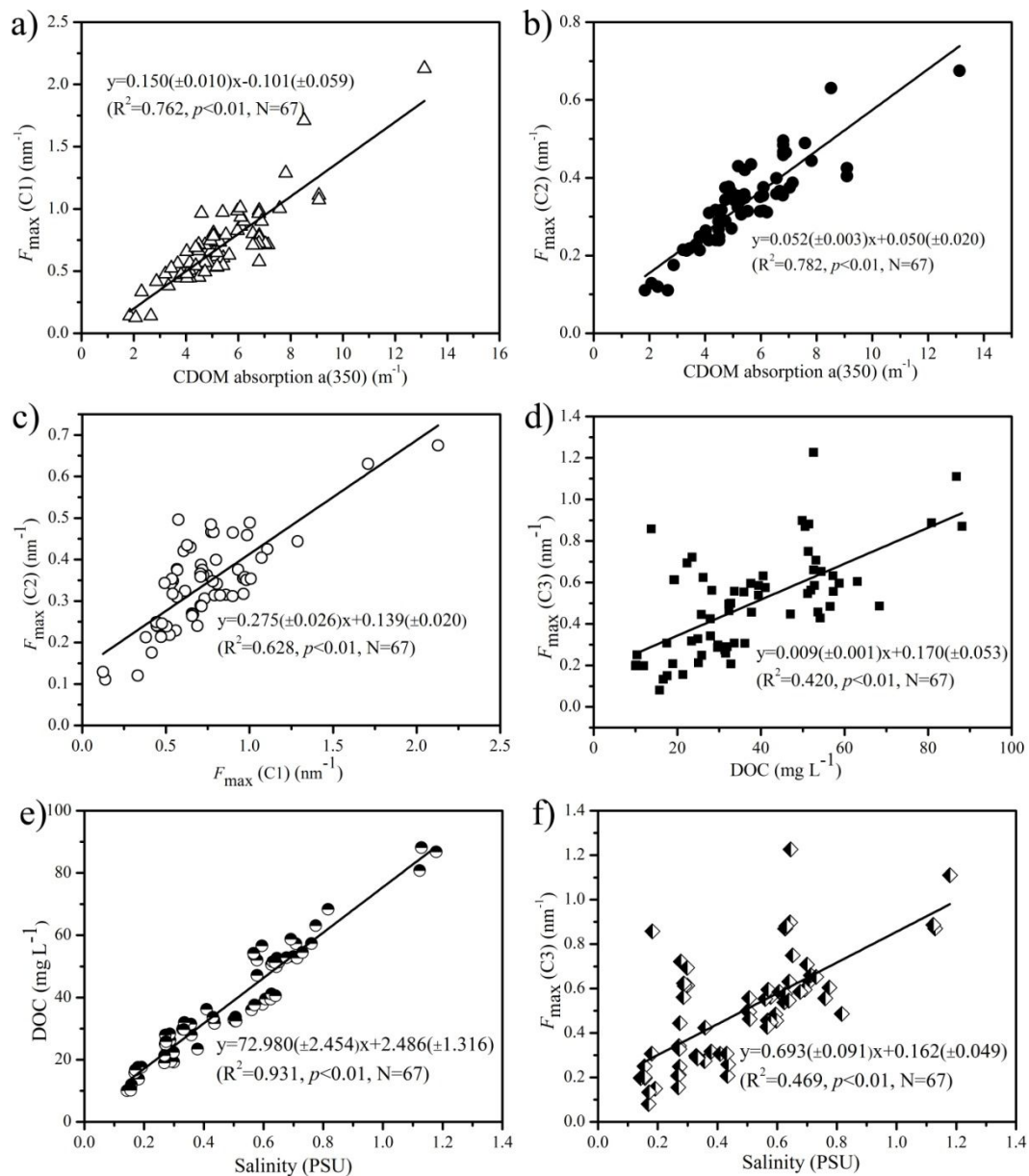
764 variation of the four EEM-PARAFAC components at different seasons. The error bars

765 represent one standard deviation.

766

767

768



769

770 Figure 4. Relationships between CDOM absorption coefficient $a(350)$ with a)

771 $F_{\max}(C1)$, b) with $F_{\max}(C2)$, c) $F_{\max}(C1)$ versus $F_{\max}(C2)$, d) $F_{\max}(C3)$ versus DOC, e)

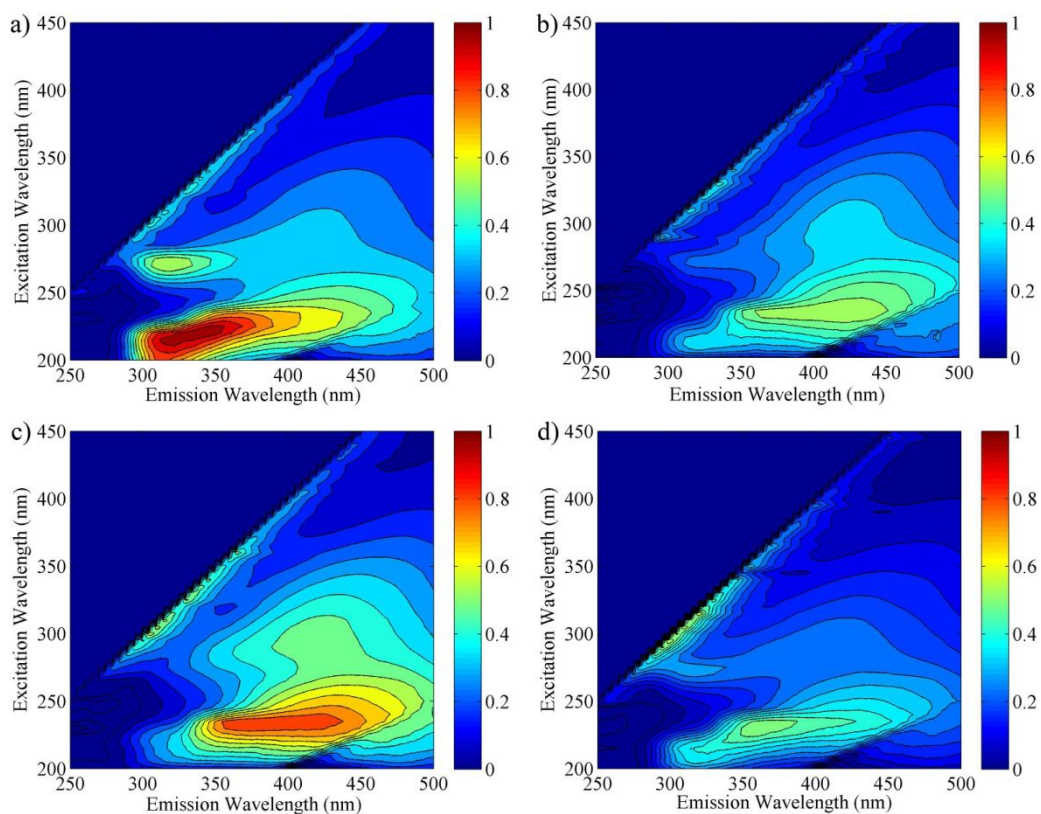
772 Salinity versus DOC, f) Salinity versus $F_{\max}(C3)$.

773

774

775

776



777

778 Figure S1. Examples of EEMs for one water sample from Xindianpao Lake in the
 779 western part of Jilin province at different seasons a) June 2013; b) August 2013; c)
 780 February 2014; d) April 2014 (Fluorescence is in Raman unit: nm^{-1}).

781

782

783

784

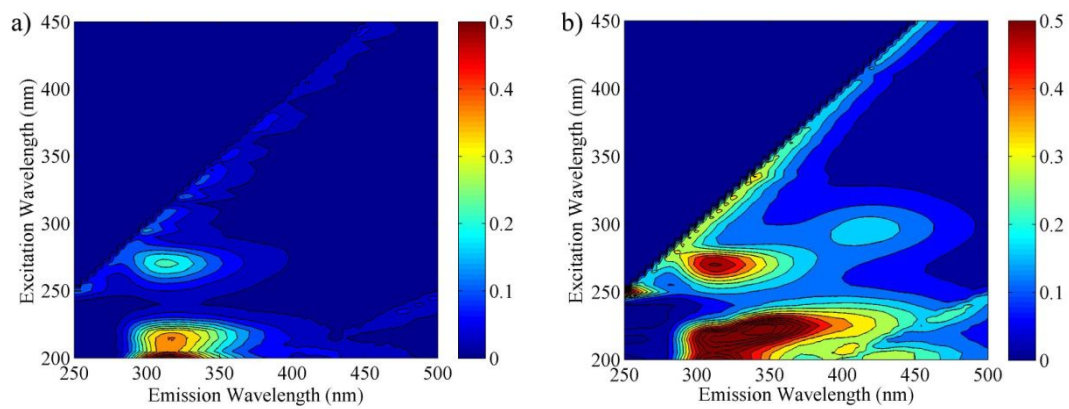
785

786

787

788

789



790

791 Figure S2. Representative examples of EEMs for a) lake ice-melt water sample, and b)

792 rainwater CDOM in the western part of Jilin province (Raman: nm^{-1}).